Controller Design of *LC*-Based Grid-Tied Converter to Guarantee Passivity Up to the Nyquist Frequency

Alvaro Morales-Muñoz, *Student Member, IEEE*, Francisco D. Freijedo, *Senior Member, IEEE*, Sante Pugliese, *Member, IEEE*, and Marco Liserre, *Fellow, IEEE*

***Abstract*—The main benefit of designing for passivity raises when passive systems are interconnected, because the resulting system is also passive and consequently globally stable. Therefore, passivity-based control design is suitable for grid-connected power electronic converters to ensure the stability also considering interactions with other power converters. However, ensuring the passive behavior of a converter up to the Nyquist frequency is challenging, mainly due to the phase shift introduced by the computation and the PWM delay at high frequencies. Previous state-of-the-art techniques face drawbacks, such as requiring extended states, which sometimes include a signal derivative, leading to noise injection, reliance on experience-based filter tuning, and/or incomplete damping of *LC*/LCL filter resonance. This article proposes a passivity-based control design achieved through proportional state feedback that avoids extended states, achieves *LC*/LCL resonance damping and delay phase-shift effect compensation around the Nyquist region. The proposal is compared with the state of the art and experimentally tested.**

***Index Terms*—DC–AC power conversion, grid-connected power converters, passivity, stability.**

I. Introduction

STABILITY of modern electrical networks is a challenge due to the interconnection of many different systems presenting high frequency dynamics. Design for passivity helps to tackle it, as the feedback interconnection of stable and passive subsystems results in a stable and passive system [1], [2], [3]. For linearized subsystems, passivity compliance is achieved when its impedance/admittance does not have a nonpositive region, i.e., its phase angle belongs to $[-90°, 90°]$ at all frequencies [1], [2]. In power electronics conversion systems, passivity is promoted by its ability to damp electrical resonances due to reactances in the grid [3]. Some stringent standards [4] choose designs based on passivity to provide stability when dealing with large electrical systems, regardless of the number of converters [3], [5]. For power electronic converters, passivity compliance at high frequencies can be seen in single-input-single-output models, and the biggest challenge comes from control action delay effects within the inner loops [3], [5].

Representative design for passivity approaches for grid-connected converters, which ideally target a wide frequency range for compliance, are compared and summarized in Table I. First, Harnefors et al. [6] proposed a composite derivative plus lead-lag filter within an active damping voltage feedback loop to account for high-frequency delay effects and then to extend the passivity compliance region up to the Nyquist frequency. Limitations of this type of approach could arise from high-frequency noise amplification and mismatch between continuous and discrete models of the feedback filter. In [7] and [8], capacitor current is measured and fed back to avoid derivative terms and reach passivity. Furthermore, the use of lead, lag or lead-lag filters can be seen as a method of dealing with parameter tolerance i.e., increasing the robustness of the design. However, the closed-loop responses remain underdamped around potential *LC* filter resonances. Similarly, the authors in [9] and [10] combined capacitor voltage and current measurements with feedback filters to obtain a passivity-based design. The drawbacks of these techniques are that they require additional sensors and part of the tuning is based on experience. The authors in [11] and [12] used a single loop to track the voltage together with a damping loop to achieve passivity using grid-side current measurement in combination with a lead-lag filter. However, the resonance due to the *LC* filter is not fully damped. A different approach is given in [13], where the authors propose to extend the passive range by using delay compensation by predicting the feedback values for the next sampling cycle. The passive behavior of this technique is limited to 0.39 of the Nyquist frequency. Beyond this frequency, the negative resistance values increase rapidly. In [14], the integral of the voltage measured at the point of connection is fed back to obtain an admittance response that corresponds to a purely inductive behavior. However, the introduction of an integral action when applied to the measured point of common coupling (PCC) voltage while the tracked variable is the current, may impact the tracking performance. Moreover, the voltage measurement may have an offset, which, in combination with the infinite gain at dc of the controller, can create a large dc bias, thus causing the malfunction of the system. The solution to these issues suggests that achieving completely passive behavior may not be feasible [14]. In a subsequent work by the same authors [15], passivity is achieved by using notch filters that narrow the control bandwidth around the fundamental

Received 3 September 2024; revised 20 December 2024; accepted 10 January 2025. Date of publication 21 January 2025; date of current version 26 February 2025. Recommended for publication by Associate Editor M. Molinas. *(Corresponding author: Alvaro Morales-Muñoz.)*

Alvaro Morales-Muñoz and Francisco D. Freijedo are with the Huawei Technologies Duesseldorf GmbH, Nuremberg Research Center, 90449 Nuremberg, Germany (e-mail: alvaro.morales.munoz@huawei.com).

Sante Pugliese and Marco Liserre are with the Chair of Power Electronics, Christian-Albrechts, University of Kiel, 24143 Kiel, Germany.

Color versions of one or more figures in this article are available at https://doi.org/10.1109/TPEL.2025.3532310.

Digital Object Identifier 10.1109/TPEL.2025.3532310

TABLE I
COMPARISON OF THE STATE-OF-THE-ART TECHNIQUES FOR PASSIVITY-BASED DESIGN

Ref.	Description	Disadvantages	Validation through impedance spectroscopy
[6]	Pioneer work. It uses a time-derivative open-loop observer for capacitor current state feedback. It includes a lead-lag filter to increase the phase angle at high frequencies to extend the passivity region.	Time derivative is sensitive to high-frequency noise. Lead-lag filters add extended states implicit. It does not account for discretization in frequency domain.	No.
[7], [8], [9], [10]	The capacitor current is measured for the state feedback to achieve passivity (time-derivative is avoided). Filters are applied to increase the robustness of the design.	Filter tunings are not straightforward and are based on the experience. *LC*/LCL filter resonances are not properly damped.	No.
[11], [12]	Passivity is achieved for a single voltage loop control by feeding the grid-side current measurement through a lead-lag filter.	Grid-side current measurement is needed. *LC*/LCL resonances are not well damped. Lead-lag filter tuning is not straightforward.	No.
[13]	Passivity is increased by delay compensation through prediction of feedback values for the next sample cycle.	The passivity range is limited to 0.39 of the Nyquist frequency. Beyond this value, the negative resistance values increase rapidly.	No.
[14], [15]	By modifications within the control loop, the control action is canceled in a wide range of frequencies, allowing the system to operate in a passive open-loop mode at such.	*LC*/LCL filters are not considered in the converter scheme. Likely, the resonance damping is not provided since the current controller sets a behavior is similar to a pure inductor.	Simulation.
[16]	Control delays are reduced by increasing the sampling frequency. The passivity range is increased accordingly.	Acquisition system complexity increases. Multisampling bandwidth is limited due to switching (sideband) noise.	Experimental.
[18]	Passivity is achieved by applying optimization in a continuous-domain model. Experimental admittance spectroscopy is provided.	The design is not heuristic and the optimization is nonsmooth, i.e., require high computational effort.	Experimental.
[19]	Passivity is achieved by solving an optimization problem, based on a continuous-domain model, where the constraints are obtained from a discrete-domain model.	The optimization problem is nonlinear, i.e., it requires high computational effort.	No.
[5]	Discrete-time methodology. Time derivative is used and a pole-zero cancellation seeks order reduction and hence passivity. Comprehensive impedance spectroscopy verification is provided.	Derivative signals may amplify noise. Discrete-time model is conservative about phase margin at high frequencies. At high frequencies, passivity relies on real losses.	Experimental.
[20], [21]	Discrete-time modeling. A full state-feedback control law without extended states is used to achieve passivity in a wide frequency range.	Passivity up to the Nyquist frequency is not guaranteed. This would require the introduction of a resistance into the *LC* filter.	[20] experimental, [21] no.

frequency. Thus, the system behaves in an open-loop mode at high frequencies. A major weakness of these approaches is that the *LC* filter is not considered in the converter model, and its resonance is unlikely to be damped due to the control bandwidth limitation. Another different approach is given in [16], where the solution to extend the passivity compliance region is to increase the sampling frequency, i.e., by multisampling. Reducing the delay effect improves the phase margins, so the passivity region is much wider. However, measuring close to the switching events can lead to the measurement of voltage and/or current ripple [17]. Another view is given in [18]. The passivity-based design is achieved through a robust controller scheme and relies on an optimization process applied to a continuous domain where the delay is approximated by Pade. As a result of the optimization problem, complex gains (i.e., coupling of orthogonal states) are obtained. The performance of this proposal is verified with an experimental admittance spectroscopy. Apart from some complexity of the approach, a main drawback associated to the optimization process is a lack of physical meaning associated to the gains. In [19] a passivity-based design is also achieved using an optimization method. In this case a continuous-domain model sets the optimization problem and a discrete-domain model is applied to establish the optimization constraints. The main drawbacks are that the optimization problem is nonlinear, which hampers its resolution, and again there is a lack of physical meaning associated with the gains. Returning to methods whose implementation is not based on optimization, the work in [5] shows that the passivity of grid-tied inverters based on a capacitor voltage derivative can be more easily achieved when evaluated from the grid-side current of an LCL filter. Its tuning is based on a double pole-zero cancellation in the discrete domain. This work shows that the Z-domain analysis tends to be conservative at high frequencies. Its solution also relies on adding some real resistance to the *LC* filter. Another discrete-time proportional state feedback control is proposed in [20], which does not use extended states (e.g., lead-lag filters). However, the passivity up to the Nyquist frequency is achieved by assuming a minimum value for the equivalent series resistance of the filter capacitor. This article [21] proposes an elaborated discrete-time full-state feedback modeling. An *ad hoc* pole location criterion is provided. It results in complex control parameters (negative sequence control is different from positive sequence control). An issue of this approach is that the voltage tracking controller must be tuned together with the passivity control law. Also, passivity is not guaranteed up to the Nyquist frequency.

This article proposes a heuristic design for passivity methodology with the peculiarity of combining the strengths of continuous-time and discrete-time models. In particular, this design targets passivity compliance up to the Nyquist frequency. The control law is described by a full state feedback and avoids complex, derivative and/or integrative terms. It also maintains the controller simple by not adding new states (i.e., extended

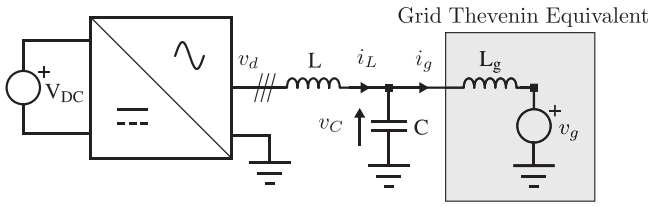

Fig. 1. Diagram of an inverter connected to the grid via an *LC* filter. The grid is represented by using the equivalent Thevenin model. The single-phase representation covers the balanced three-phase three-wire case with $\alpha\beta$-frame model [23].

states). Another advantage is that this proposal does not require multi-sampling, thus avoiding possible switching ripple injection. Furthermore, damping of *LC*/LCL filter resonances can be achieved without physical resistances under high-bandwidth conditions. Finally, this technique can be used in conjunction with a resonant controller that allows for tracking of voltage or current references. In this case, the power converter can be modeled either as a voltage or a current source (CS) equivalent [22]. Moreover, since the resonant controller operates only within a narrow frequency range, specifically around the nominal frequency, it does not interfere with the wide bandwidth response.

The rest of this article is organized as follows. Section II describes the system and control laws in discrete and continuous domains. Then, the proposed method for passivity compliance is explained in Section III-A. In Section IV, the proposed method is and compared to the state-of-the-art technique by simulation. Experimental impedance spectroscopy results of the proposal are obtained and analyzed in Section V. Finally, Section VI concludes this article.

II. System Description

A. Discrete Domain Modeling

A three-phase, three-wire, grid-tied inverter with an output symmetric *LC* filter, which is fed by an infinite power dc voltage source, is depicted in Fig. 1. In this way, a controller can be designed, specifically for voltage control [11], [20], [21], [24], [25], [26], [27], [28]. Assuming a symmetrical and balanced three-phase system, the modeling and analysis can be reduced to that of a single-phase system. A single-phase continuous-domain delay-less dynamic state–space model of the grid-tied inverter is the following, where the exogenous disturbance is a CS [24], [28] that represents the load demand, thus respecting in this way the principles of causal systems [29]:

$$\begin{aligned}\frac{di_L(t)}{dt} &= -\frac{v_C(t)}{L} + \frac{v_{\text{in}}(t)}{L}\\ \frac{dv_C(t)}{dt} &= \frac{i_L(t)}{C} - \frac{i_g(t)}{C}\end{aligned} \tag{1}$$

where i_L is the current of the inverter-side inductor, v_C is the voltage drop in the capacitor leg, v_{in} is the inverter voltage, and i_g is the grid-side current. These equations are suitable for modeling the system in the $\alpha\beta$-frame

The zero-order hold (ZOH) discretization and the addition of the delay due to the use of a digital controller can be found in [20] and [21], which follow [30] guidelines. The final state–space representation is given by (2) (show at the bottom of the next page), where

$$\begin{aligned}a &= \cos\left(\frac{T_s}{\sqrt{LC}}\right)\\ b &= \sqrt{\frac{C}{L}}\sin\left(\frac{T_s}{\sqrt{LC}}\right)\\ c &= \sqrt{\frac{L}{C}}\sin\left(\frac{T_s}{\sqrt{LC}}\right)\end{aligned} \tag{3}$$

with T_s being the sampling period. The proposed state-feedback control law is described by

$$v_{\text{in}}(z) = -\underbrace{\begin{bmatrix}K_I & K_V & K_d\end{bmatrix}}_{K}\begin{bmatrix}i_L(z) & v_C(z) & v_d(z)\end{bmatrix}^T. \tag{4}$$

B. Continuous Domain Modeling

The ZOH discretization method takes into account the digital delays, introduces the delayed action as a state [30], and preserves the position of the poles [31]. These properties are very convenient for zero-pole placement designs. However, it does not provide an accurate model of the system at high frequencies and establishes that the system cannot be passive [21], [32], [33]. ZOH transfer functions are of relative order one or higher in the Z-domain, which means that each stable pole/zero introduces a $\pm 180^\circ$ phase shift at the Nyquist frequency and compromises the passivity criterion [32], [33]. Passivity is then proved by applying a less restrictive and more accurate continuous domain model, which also includes the ZOH sampling and digital controller delay effects [16], [18], [21], [34]. First, (1) is represented in the Laplace domain

$$\begin{aligned}si_L(s) &= -\frac{v_C(s)}{L} + \frac{v_{\text{in}}(s)}{L}\\ sv_C(s) &= \frac{i_L(s)}{C} - \frac{i_g(s)}{C}.\end{aligned} \tag{5}$$

Then, the control law for passivity plus the delay are applied

$$G_{\text{ZOH}}(s) = \underbrace{\frac{1-e^{-T_s s}}{T_s s}}_{\text{ZOH delay}} \tag{6a}$$

$$G_{dd}(s) = \underbrace{e^{-T_s s}}_{\text{Dig. ctrl. delay}} \tag{6b}$$

$$G_d(s) = \frac{G_{dd}(s)G_{\text{ZOH}}(s)}{1 + K_d G_{dd}(s)} \tag{6c}$$

$$v_{\text{in}}(s) = -G_d(s)(K_I i_L(s) + K_V V_C(s)). \tag{6d}$$

It is important to note that the ZOH model considered here, (6a), while more accurate than the discrete model, assumes an ideal modulator. More refined models have been developed, such as those presented in [35] and [36]. These advanced models may also be employed as alternatives to (6a).

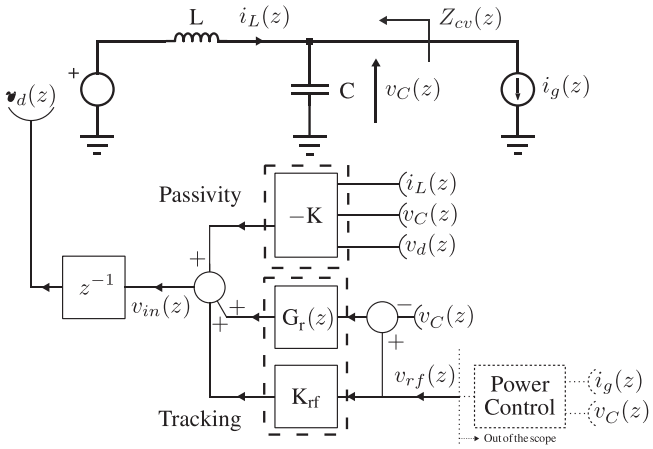

Fig. 2. Single phase model of the inverter considered and control schematic at normal operation mode of the proposed controller. The impedance of the system at PCC, Z_{cv}, is marked.

III. Controller Design

The proposed control diagram is presented in Fig. 2. A passivity-based state feedback is presented in the first part. The second part explains a selective controller for reference voltage tracking, which is commonly the output of grid-forming controllers. They rely on external loops based on active and reactive power for synchronization purpose and voltage regulation, respectively [37]. However, the influence of external loops is beyond the scope of this article, as they only affect a low frequency range.

A. Design for Passivity

The passivity compliance of the inverter can be achieved by using the converter current $i_L(z)$, the capacitor voltage $v_C(z)$, and the delayed (voltage) action $v_d(z)$, cf., Fig. 2. The goal of the passivity design is to preserve the impedance response of the converter between $+90°$ and $-90°$ [1], [2].

The design is based on a zero and pole placement criterion that attempts to bend the frequency away from $\pm 90°$at high frequencies. The impedance of the Thevenin equivalent of the converter transfer function in the Z-domain is considered

$$-Z_{\text{cv}}(z) = \frac{v_C(z)}{i_g(z)} = \begin{bmatrix} 0 & 1 & 0 \end{bmatrix} (zI - \phi^d + \Gamma_1^d K)^{-1} \Gamma_2^d \quad (7)$$

where I means the identity matrix. The expanded equation obtained by substitution of the variables, (2) and (4), in (7) is shown in (8) shown at the bottom of the next page. The poles of (8) can be divided into a real pole, p_1 and a complex pair of poles, $p_{2,3}$

$$z^3 + (K_d - 2a)z^2 + (bK_I + (1-a)K_V - 2aK_d + 1)z - bK_I + (1-a)K_V + K_d = (z+m)(z^2 + hz + n). \quad (9)$$

The impedance transfer function numerator of (8) consists of a couple of zeros, $z_{1,2}$, which do not depend on K_V. In other words, the zeros depend mostly on the inductor of the plant and the states associated with it. The frequency and damping can be obtained by $z_{1,2} = e^{(-\zeta\omega T_s \pm \omega T_s \sqrt{1-\zeta^2} j)}$

$$z^2 + (K_d - 1)z + \frac{2(1-a)}{c} K_I - K_d = z^2 - 2e^{-\zeta_z \omega_z T_s} \cos\left(\omega_z T_s \sqrt{1-\zeta_z^2}\right) z + e^{-2\zeta_z \omega_z T_s} \quad (10)$$

where ζ_z is the damping factor of the zeros and ω_z is the frequency of the zeros. Therefore, using (9) and (10), the gains can be defined as a function of m, which, eventually, is the real pole $p_1 = -m$, and the natural frequency and damping factor of the zeros

$$K_I = \frac{c}{2(1-a)} \left(e^{-2\zeta_z \omega_z T_s} + K_d\right) \quad (11a)$$

$$K_V = \frac{-1 - 2am - m^2 + (2a + m + \frac{1}{m})K_d - b(1 + \frac{1}{m})K_I}{(1-a)(1-\frac{1}{m})} \quad (11b)$$

$$K_d = 1 - 2e^{-\zeta_z \omega_z T_s} \cos\left(\omega_z T_s \sqrt{1-\zeta_z^2}\right). \quad (11c)$$

Considering three control gains and five roots (three poles and two zeros), this is an overdetermined system, which is solved by following an holistic approach that also considers the continuous domain equations.

Focusing on (6c), it is clear that K_d has a large influence on the effect of the delay over the system. This is studied by substituting a set of values in (6c), whose frequency response is depicted in Fig. 3. The main conclusion is that a large value of K_d helps to reduce the phase shift introduced by the delay. Because of the relationship between the zeros and K_d, a way to ensure a large value of K_d, but keeping the zeros inside the unit circle, has been found by selecting the frequency of the zeros as the Nyquist frequency. The damping factor values are inside the range 0 and 1, which leads to $0.96 \leq K_d \leq 3$, according to (11c).

Finally, the selection of m is examined, which affects the position of all the poles

$$p_{2,3} = -\frac{h}{2} \pm \sqrt{\frac{h^2}{4} - n}. \quad (12)$$

$$z \begin{bmatrix} i_L(z) \\ v_C(z) \\ v_d(z) \end{bmatrix} = \underbrace{\begin{bmatrix} a & -b & b \\ c & a & 1-a \\ 0 & 0 & 0 \end{bmatrix}}_{\phi^d} \begin{bmatrix} i_L(z) \\ v_C(z) \\ v_d(z) \end{bmatrix} + \underbrace{\begin{bmatrix} 0 \\ 0 \\ 1 \end{bmatrix}}_{\Gamma_1^d} v_{\text{in}}(z) + \underbrace{\begin{bmatrix} 1-a \\ -c \\ 0 \end{bmatrix}}_{\Gamma_2^d} i_g(z). \quad (2)$$

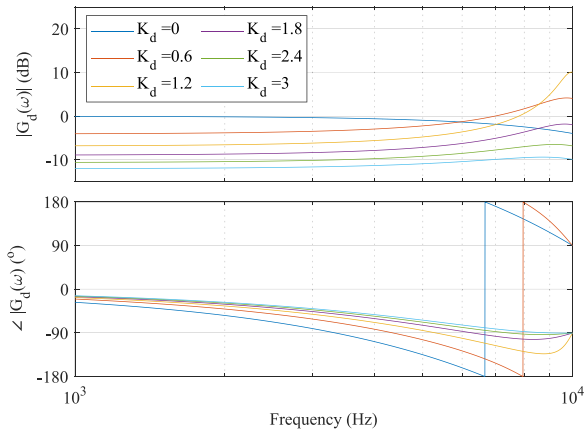

Fig. 3. Effect of the gain K_d over the delay.

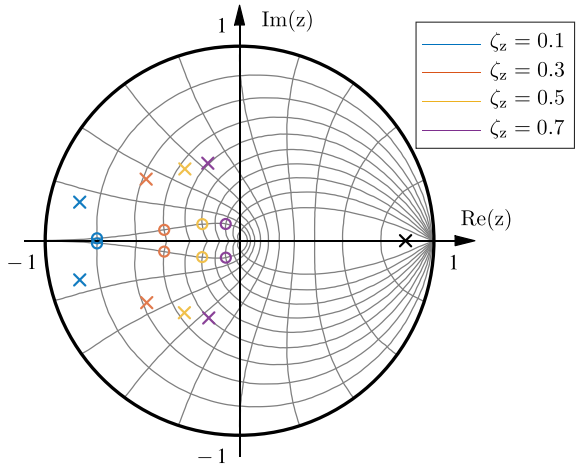

Fig. 4. Poles and zeros location of the impedance Z_{CV} depending on the damping factor of the complex zeros when the single pole is located at 500 Hz, $-m = e^{-2\pi 500 T_s}$, and the natural frequency of the zeros is at Nyquist frequency, $\omega_z = \frac{2\pi}{2T_s}$.

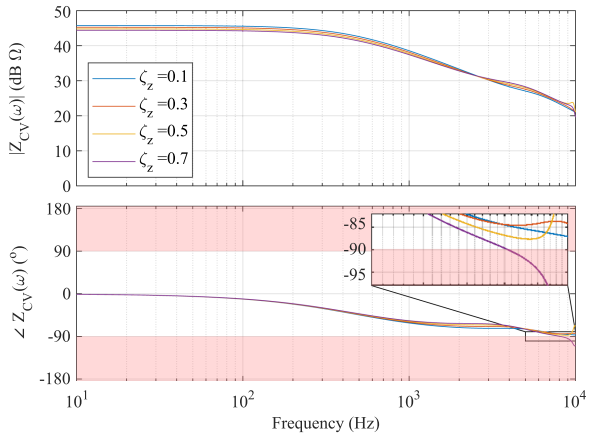

Fig. 5. Frequency response of the impedance Z_{CV} depending on the damping factor of the complex zeros when the single pole is located at 500 Hz, $-m = e^{-2\pi 500 T_s}$, and the natural frequency of the zeros is at Nyquist frequency, $\omega_z = \frac{2\pi}{2T_s}$.

The real part of the complex poles is given by $\text{Re}(p_{2,3}) = -\frac{h}{2} = \frac{2a+m-K_d}{2}$. The expression of the $\text{Re}(p_{2,3})$ implies that lowering the frequency of the real pole p_1 causes the complex pole pair $p_{2,3}$ to shift further to the left side of the unit circle.

The first constraint is that p_1 must lie within the unit circle on the positive real axis, which implies that $-1 \leq m \leq 0$. In addition, the complex poles $p_{2,3}$ should be close in frequency to the complex zeros

$$z_{1,2} = \frac{1-K_d}{2} \pm \sqrt{\frac{(K_d+1)^2}{4} - \frac{2(1-a)K_I}{c}} \tag{13}$$

which are located at a high frequency and are independent of m. This condition ultimately results in the damping of the *LC* filter resonance through the pole-zero cancellation of $p_{2,3}$ with $z_{1,2}$. Comparing the real part of $p_{2,3}$ and $z_{1,2}$, a second constraint on m can derived as $m \leq 1-2a$. Moreover, the interaction between complex poles and the real pole should be avoided, i.e., they should be decoupled (at least a frequency difference of five times [30]). Assuming this decoupling, p_1 becomes the dominant pole, leading to the third design constraint. A higher frequency for p_1 is preferred to ensure a wider predominantly resistive behavior, without affecting the performance of reference tracking and disturbance rejection controllers, around nominal frequency (at least a frequency difference of five times [30]). Combining all the constraints a region of design for m emerges

$$-e^{5\omega_0 T_s} \leq m \leq 1-2a \tag{14}$$

where w_0 is the nominal frequency.

Stability robustness, i.e., goodness of the tuning, should consider the position of the zeros and poles of (8) (cf., Fig. 4 for different design values) and the high frequency response from the continuous model. By combining (5) and (6), the continuous-model impedance transfer function is given by

$$\begin{aligned} Z_{\text{cv}}(s) &= -\frac{v_C(s)}{i_g(s)} \\ &= \frac{\frac{1}{C}s + \frac{K_I G_d(s)}{LC}}{s^2 + \frac{K_I G_d(s)}{L}s + \frac{1+K_V G_d(s)}{LC}}. \end{aligned} \tag{15}$$

Its frequency response is used to check the passivity in the high frequency range, e.g., as shown in Fig. 5 for different damping factors. A quick checking about the tuning can be extracted from the necessary condition obtained by $Z_{\text{cv}}(s=0) \geq 0$, assuming

$$-Z_{\text{cv}}(z) = \frac{-c\left(z^2 + (K_d-1)z + \frac{2(1-a)}{c}K_I - K_d\right)}{z^3 + (K_d-2a)z^2 + (bK_I + (1-a)K_V - 2aK_d + 1)z - bK_I + (1-a)K_V + K_d} \tag{8}$$

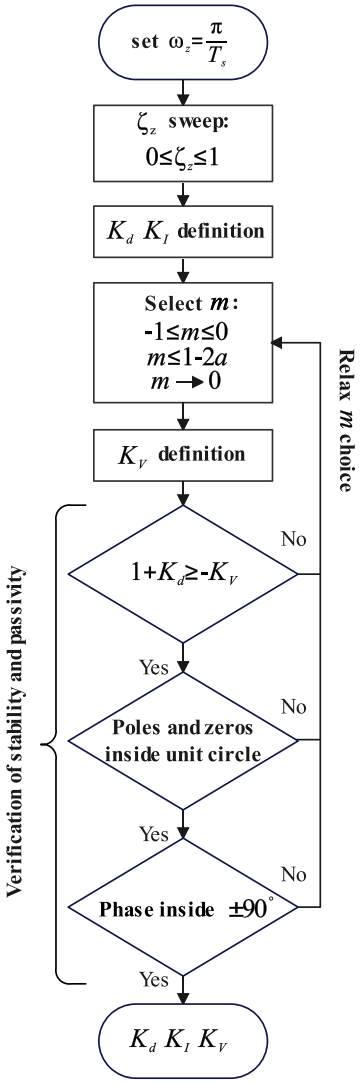

Fig. 6. Passivity-based tuning proposal diagram.

$K_I \geq 0$, which is

$$1 + K_d \geq -K_V. \tag{16}$$

The proposed tuning methodology described in this section is summarized in Fig. 6.

B. Signal Tracking

The tracking controller should not change the base behavior achieved with the passivity controller. For this reason, a resonant filter is chosen

$$G_r(s) = \frac{K_a s + K_b}{s^2 + \omega_0^2}. \tag{17}$$

It changes the main behaviour in a narrow frequency range, where it provides a high gain, and then achieves perfect reference tracking and disturbance rejection in steady state. It should be tuned for the expected range of short circuit ratio [31], [38]. A strategy for reducing the harmonics content in a specific variable, i.e., voltage or current, is to feed back the variable measurement after filtering it through resonant controllers at the desired frequencies [19], [31], [38]. Equation (17) can be discretized by applying zero-pole matching as

$$G_r(z) = \frac{K_2 z + K_1}{z^2 - 2\cos(\omega_0 T_s) z + 1}. \tag{18}$$

The design is oriented for tracking voltage, but similar deductions can be made for tracking current. A feedforward term, K_{rf}, is added to the resonant controller for improving the transient

$$\begin{aligned} v_{\text{in}}(z) = &-K_I i_L(z) - K_d v_d(z) - K_V v_C(z) \\ &+ G_r(z)\left(v_{\text{rf}}(z) - v_C(z)\right) + K_{\text{rf}} v_{\text{rf}}(z). \end{aligned} \tag{19}$$

In principle, the feedforward term is not strictly needed to reach steady-state performances. The criterion to calculate the gain of the feedforward gain is done by achieving perfect tracking at dc without considering the disturbance, i.e., substituting (19) in (2)

$$\left.\frac{v_C(z=1)}{v_{\text{rf}}(z=1)}\right|_{i_g=0} = 1 \Rightarrow K_{\text{rf}} = 1 + K_d + K_V. \tag{20}$$

Similar input can be applied to the continuous domain model

$$\begin{aligned} v_{\text{in}}(s) = &-G_d(s)(K_I i_L(s) + K_V v_C(s) \\ &+ G_r(s)\left(v_C(s) - v_{rf}(s)\right) - K_{\text{rf}} v_{\text{rf}}(s)). \end{aligned} \tag{21}$$

C. Robustness Against Filter Parameter Tolerance

The values of the filter components are not always precisely known, or sometimes even unknown; suppliers always provide a tolerance, and these component values can vary with operating factors or conditions, such as operating temperature, voltage level, or supplied power. This section discusses the effect of the design decision as a function of parameter variability.

If a low-damping factor is chosen, $\zeta_z = 0.1$, the passivity is always maintained in the considered cases, cf., Figs. 7 and 8. However, in terms of stability, increasing the inductance by 10 % produces the system to become unstable, while a decrease of a 10% in the inductance places the system near the edge, but again on the side of instability, cf., Fig. 7. If a high-damping factor, which allows the passivity, is chosen, $\zeta_z = 0.5$, the system maintains the stability. Nevertheless, the passivity is at the edge when the inductance is increased, cf., Fig. 7. With the same variations in the capacitance of the filter, it can be appreciated that it has less influence in the zero-pole location in any case, but in the case of high damping, the passivity can be broken, cf., Fig. 8.

IV. Simulation Results

The proposed method is compared with the work proposed in [21]. The parameters of the system and the control gains appear in Table II. After the previous considerations, the single pole location at 500 Hz, $m = -e^{-2\pi 500 T_s} \approx -0.85$, $\omega_z = \frac{2\pi}{2T_s}$, and $\zeta_z = 0.3$ is found as a design that maintains the stability and passivity against filter parameters drift. This means more than 5° phase margin to -90° with nominal parameters and a radius of the complex poles of, approximately, 0.465.

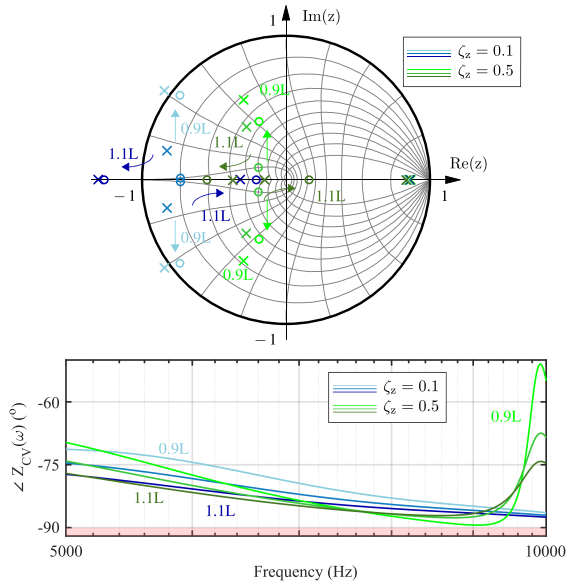

Fig. 7. Poles and zeros location, and phase response of the impedance Z_{CV} depending on the inductance variation of the *LC* filter when $-m = e^{-2\pi 500 T_s}$, $\omega_z = \frac{2\pi}{2T_s}$, and $\zeta_z = 0.1$ or $\zeta_z = 0.5$.

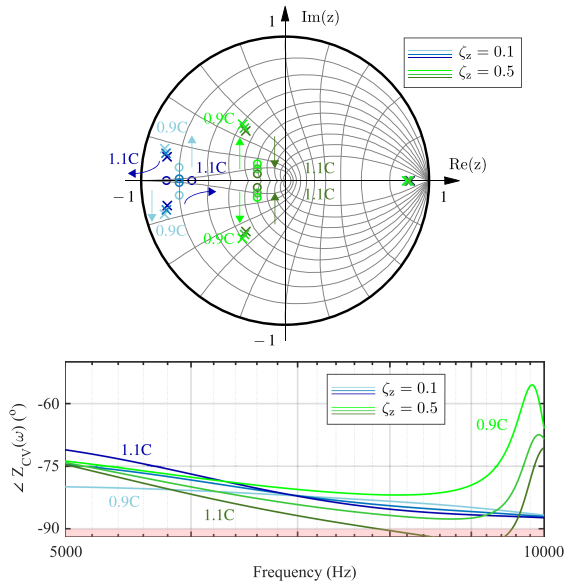

Fig. 8. Poles and zeros location, and phase response of the impedance Z_{CV} depending on the capacitance variation of the *LC* filter when $-m = e^{-2\pi 500 T_s}$, $\omega_z = \frac{2\pi}{2T_s}$, and $\zeta_z = 0.1$ or $\zeta_z = 0.5$.

TABLE II
PARAMETERS AND CONTROLLER GAINS VALUES

Param.	Value	Gain	Value	Gain	Value
L	5.0 mH	K_I	187	K_I	$36.2 + 1.95j$
C	1.5 μF	K_V	-1.75	K_V	$-0.693 + 0.028j$
L_g	1.0 mH	K_d	1.77	K_d	$0.468 + 0.0157j$
f_{sp}	20 kHz	K_1	-0.1	K_r	$-1640 - 242j$
f_{sw}	10 kHz	K_2	0.10003	ω_i	$2\pi 3$ rad/s
S_b	4 kVA	K_{rf}	1.02	α_1	1
V_b	400 V	ω_0	$2\pi 50$ rad/s	ω_{c1}	$0.01\omega_0$ rad/s
Z_b	40 Ω	Control ⇑		Control [21] ⇑	

Hardware ⇑

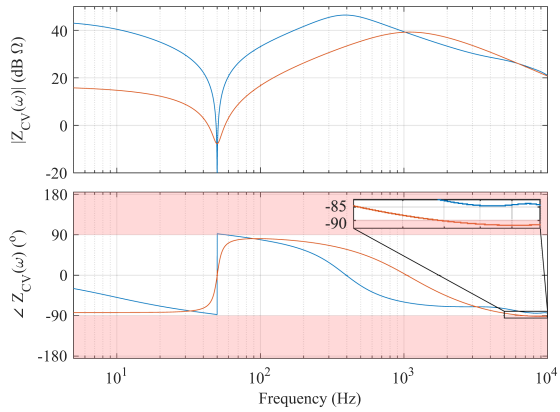

Fig. 9. Frequency impedance response of the work presented in [21], in orange, compared to this article approach passivity-based method, in blue. Passivity is not achieved in [21] case because the phase angle crosses $+90°$ or $-90°$.

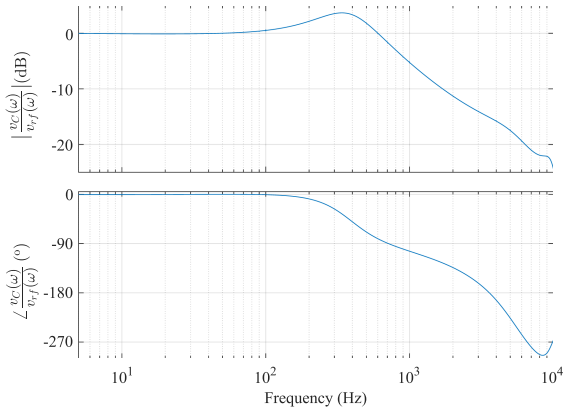

Fig. 10. Frequency response of the closed-loop transfer function $\frac{v_C(s)}{v_{rf}(s)}$.

A. *Impedance Frequency Response*

Substituting the gains into (15) and applying a frequency sweep, gives Fig. 9, which is the frequency response of the impedance of the system. It can be seen that our proposal keeps the passivity along all the bandwidth. On the other hand, the method of [21] cannot ensure the passive behavior. In this case, it is slightly nonpassive at high frequencies. At low frequency, [21] impedance is much lower thanks to the use of a complex resonant filter. It tracks only the positive sequence. However, the response of the system in this range is dominated by the power loops. Therefore, a high absorption of subharmonics waveform is not guaranteed. This also means that negative sequence disturbances at nominal frequency are not rejected.

In both cases, the resonance is damped and both sequences of the fundamental frequency are under control. The high-frequency harmonic rejection terms are neglected in this comparison because they do not affect it.

B. *Voltage Tracking*

Combining (5), (6) and the input, (21), the closed-voltage loop transfer function, $\frac{v_C(s)}{v_{rf}(s)}$, is extracted and its frequency response is illustrated in Fig. 10.

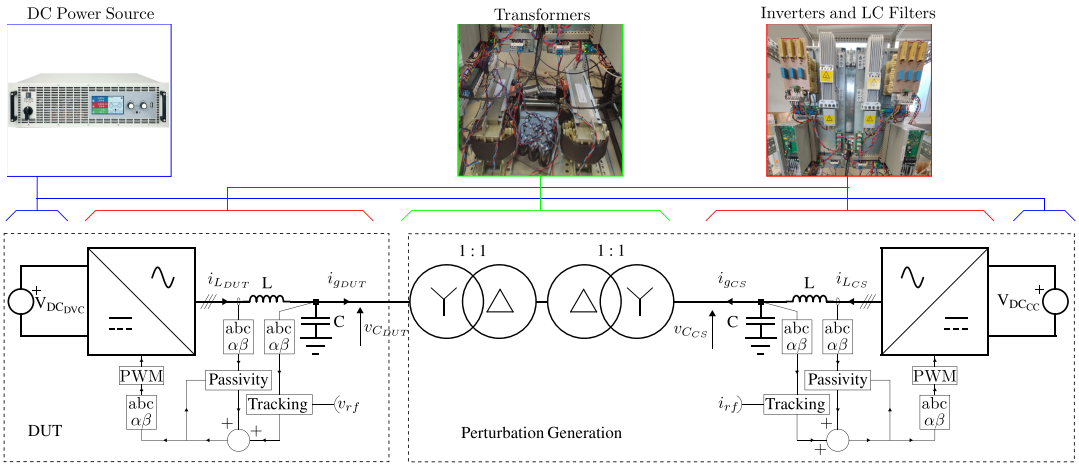

Fig. 11. Setup schematic of two inverters in parallel for output impedance identification: one acts as a voltage source (DUT), and other such as a CS (disturbance generation).

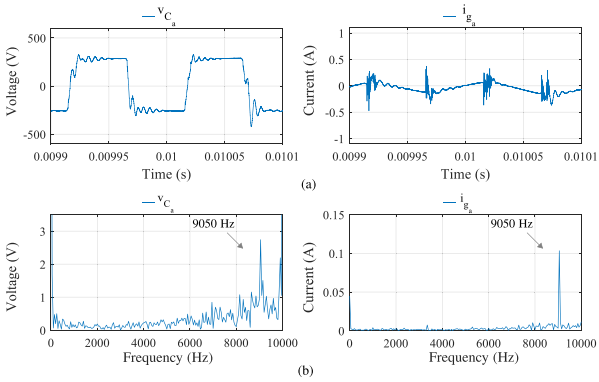

Fig. 12. Example of an experimental measurement for identification of the impedance response in the harmonic 181 (9050 Hz). (a) Time-domain waveforms including the 9050 Hz grid-side current disturbance and capacitor leg voltage response. (b) Amplitude of the waveforms obtained by applying FFT. Special relevance of the peaks at 9050 Hz.

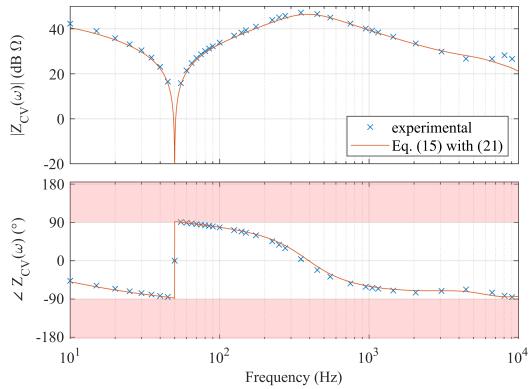

Fig. 13. Impedance spectroscopy (frequency impedance response) of the ZOH discrete domain model and experimental data. Passivity is achieved because the phase angle never crosses $+90°$ or $-90°$ (red area). At nominal frequency (50 Hz) the gain does not appear because it was too low value.

The voltage reference is perfectly tracked at nominal frequency, where the resonant filter dominate the system response.

V. Experimental Results

The experiments were carried on using inverters Danfoss FC-302, and their filters, as shown in Fig. 11. The values of parameters are collected in Table II. The control method is implemented in a dSpace real-time fast prototyping control board. Synchronous sampling and double update is used. Measurements are recorded by a Lecroy HDO6104-MS oscilloscope with a sampling frequency of 1.25 MHz.

A. Output Impedance Measurement

This test is performed using two similar inverters connected in parallel, as shown Fig. 11. One of them controls the voltage, device under test (DUT) (see Table II), which acts as a voltage source, and the second one controls the current, which operates as a CS that permits to inject very high-frequency currents. The current controlled inverter generates the disturbance input of the

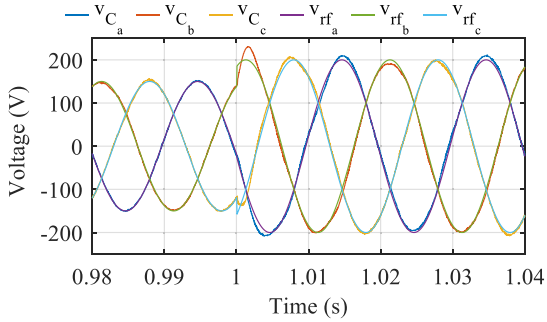

Fig. 14. Time domain response of a voltage reference step, from 150 to 200 V, at $t = 1$s.

DUT. For this reason, a controller with very high bandwidth and proper stability is needed. In fact, the current controller of the CS inverter is mostly based on proportional gains [same control law for the passivity-based proposed design and a feedforward term with a proportional gain calculated similarly as in (20)]. Thus, the tracking of the amplitude and phase is not perfect, but the main objective is to inject high-frequency current and achieve a

wide bandwidth, which is fulfilled. The amplitude of the injected signal is not relevant because the presented controller is fully linear.

In other words, injecting a current with a specific frequency, that is measured by the oscilloscope, into the system will release a response in the target system that can be measured by the oscilloscope in the capacitor leg voltage with the same frequency to identify the impedance, cf., Fig. 12(a). By using the FFT (e.g., from the oscilloscope output [39], [40]), the amplitude and phase of the impedance can be obtained, cf., Fig. 12(b), from the expressions

$$|Z_{\text{cv}}(j\omega)| = \frac{|v_{C_{\text{DUT}}}(j\omega)|}{|i_{g_{\text{DUT}}}(j\omega)|}$$
$$\angle Z_{\text{cv}}(j\omega) = \angle v_{C_{\text{DUT}}}(j\omega) - \angle i_{g_{\text{DUT}}}(j\omega). \tag{22}$$

As the output voltage also depends on the reference signal, $v_{\text{rf}} = 0$.

The result, Fig. 13, shows that passivity is satisfied in the full range of the measurement setup. Moreover, the effect of the resonant filter is clear due to the low gain around the nominal frequency. Passivity constraints are met.

B. Voltage Tracking Dynamic

This experiment aims to evaluate the dynamic performance of the controller by applying a step change to the voltage reference. To this end, two similar inverters are connected in parallel, as shown Fig. 11. The inverter that emulates the perturbation acts as a CS and maintains constant the current, while the voltage reference of the DUT is varied from 150 to 200 V at $t = 1$s, as shown in Fig. 14.

The response is dominated by the action of the resonant controller and exhibits an underdamped behavior, which is intrinsic to the resonant filter [41]. Finally, the steady-state error is zero due to the infinite gain at the nominal frequency of the resonant controller.

VI. Conclusion

This article proposes a heuristic design for passivity method for the control of grid-tied inverters. The control law is based on state-feedback and does not require extended states and complex gains. The method combines pole placement in the Z-domain model, with decisions based on physical findings, i.e., delay compensation at high frequencies by properly choosing K_d. The accuracy of the continuous-domain model is also taken into account to prove passivity from the low-frequency range up to the Nyquist frequency. In addition, the system attenuates *LC* resonances through double pole-zero cancellation. This design, which has been developed for a three-phase balanced system, applies to a single phase case.

In addition, the passivity-based control design is accompanied by a resonant filter for tracking the 50 Hz component without compromising passivity in any other frequencies.

Finally, the robustness of the method against filter parameter variability is demonstrated. For the selected case, a phase margin of 5° respect to -90° is achieved and a radius of the most sensitive poles to parameter variation of 0.435. Experimental verification is based on an impedance spectroscopy test that validates the accuracy and performance of the proposed method.

References

[1] J. Bao and L. Peter, *Process Control: The Passive Systems Approach*. Berlin, Germany: Springer, 2007.

[2] J. Slotine and W. Li, *Applied Nonlinear Control*. Englewood Cliffs, NJ, USA: Prentice-Hall, 1991.

[3] L. Harnefors, X. Wang, A. G. Yepes, and F. Blaabjerg, "Passivity-based stability assessment of grid-connected VSCs—An overview," *IEEE Trans. Emerg. Sel. Topics Power Electron.*, vol. 4, no. 1, pp. 116–125, Mar. 2016.

[4] *CENELEC - EN 50388 Railway Appl. - Power supply and rolling stock - Tech. criteria for the coordination between power supply (substation) and rolling stock to achieve interoperability*, Mar. 2012.

[5] E. Rodriguez-Diaz, F. D. Freijedo, J. M. Guerrero, J.-A. Marrero-Sosa, and D. Dujic, "Input-admittance passivity compliance for grid-connected converters with an LCL filter," *IEEE Trans. Ind. Electron.*, vol. 66, no. 2, pp. 1089–1097, Feb. 2019.

[6] L. Harnefors, A. G. Yepes, A. Vidal, and J. Doval-Gandoy, "Passivity-based controller design of grid-connected VSCs for prevention of electrical resonance instability," *IEEE Trans. Ind. Electron.*, vol. 62, no. 2, pp. 702–710, Feb. 2015.

[7] A. Akhavan, S. Golestan, J. C. Vasquez, and J. M. Guerrero, "Passivity enhancement of voltage-controlled inverters in grid-connected microgrids considering negative aspects of control delay and grid impedance variations," *IEEE Trans. Emerg. Sel. Topics Power Electron.*, vol. 9, no. 6, pp. 6637–6649, Dec. 2021.

[8] X. Wang, Y. He, D. Pan, H. Zhang, Y. Ma, and X. Ruan, "Passivity enhancement for LCL-filtered inverter with grid current control and capacitor current active damping," *IEEE Trans. Power Electron.*, vol. 37, no. 4, pp. 3801–3812, Apr. 2022.

[9] C. Xie, K. Li, J. Zou, and J. M. Guerrero, "Passivity-based stabilization of LCL-type grid-connected inverters via a general admittance model," *IEEE Trans. Power Electron.*, vol. 35, no. 6, pp. 6636–6648, Jun. 2020.

[10] Y. Zhao, C. Xie, C. Peng, and J. Zou, "Passivity-based design of frequency adaptive repetitive controller for LCL-type grid-connected inverters," *IEEE Trans. Power Electron.*, vol. 39, no. 4, pp. 4017–4028, Apr. 2024.

[11] G. Wu et al., "Passivity-based stability analysis and generic controller design for grid-forming inverter," *IEEE Trans. Power Electron.*, vol. 38, no. 5, pp. 5832–5843, May 2023.

[12] A. Akhavan, J. C. Vasquez, and J. M. Guerrero, "Passivity-based control of single-loop grid-forming inverters," *IEEE J. Emerg. Sel. Topics Ind. Electron.*, vol. 4, no. 2, pp. 571–579, Apr. 2023.

[13] M. Miranbeigi, P. M. Gajare, J. Benzaquen, P. Kandula, and D. Divan, "On the passivity of grid-forming converters — role of virtual impedance," in *Proc. IEEE Appl. Power Electron. Conf. Expo.*, 2022, pp. 650–656.

[14] H. Wu and X. Wang, "Virtual-flux-based passivation of current control for grid-connected VSCs," *IEEE Trans. Power Electron.*, vol. 35, no. 12, pp. 12673–12677, Dec. 2020.

[15] H. Wu and X. Wang, "Passivity-based dual-loop vector voltage and current control for grid-forming VSCs," *IEEE Trans. Power Electron.*, vol. 36, no. 8, pp. 8647–8652, Aug. 2021.

[16] I. Z. Petric, P. Mattavelli, and S. Buso, "Passivation of grid-following VSCs: A comparison between active damping and multi-sampled PWM," *IEEE Trans. Power Electron.*, vol. 37, no. 11, pp. 13205–13216, Nov. 2022.

[17] L. Corradini, P. Mattavelli, E. Tedeschi, and D. Trevisan, "High-bandwidth multisampled digitally controlled DC–DC converters using ripple compensation," *IEEE Trans. Ind. Electron.*, vol. 55, no. 4, pp. 1501–1508, Apr. 2008.

[18] J. Serrano-Delgado, S. Cobreces, M. Rizo, and E. J. Bueno, "Low-order passivity-based robust current control design for grid-tied VSCs," *IEEE Trans. Power Electron.*, vol. 36, no. 10, pp. 11886–11899, Oct. 2021.

[19] C. Gao et al., "Passivity-based optimal state-feedback control for LCL-filtered grid-following converter," *IEEE Trans. Power Electron.*, vol. 39, no. 10, pp. 13009–13022, Oct. 2024.

[20] A. M. Munoz, F. D. Freijedo, S. Pugliese, and M. Liserre, "A passivity-based high-bandwidth voltage control for grid-forming inverters," in *Proc. IEEE 13th Int. Symp. Power Electron. Distrib. Gener. Syst.*, 2022, pp. 1–6.

[21] H. Yu, M. A. Awal, H. Tu, Y. Du, S. Lukic, and I. Husain, "Passivity-oriented discrete-time voltage controller design for grid-forming inverters," in *Proc. IEEE Energy Convers. Congr. Expo.*, 2019, pp. 469–475.

[22] J. Sun, "Impedance-based stability criterion for grid-connected inverters," *IEEE Trans. Power Electron.*, vol. 26, no. 11, pp. 3075–3078, Nov. 2011.

[23] L. Antonio de Souza Ribeiro, F. D. Freijedo, F. de Bosio, M. Soares Lima, J. M. Guerrero, and M. Pastorelli, "Full discrete modeling, controller design, and sensitivity analysis for high-performance grid-forming converters in islanded microgrids," *IEEE Trans. Ind. App.*, vol. 54, no. 6, pp. 6267–6278, Nov./Dec. 2018.
[24] V. Pirsto, J. Kukkola, and M. Hinkkanen, "Multifunctional cascade control of voltage-source converters equipped with an LC filter," *IEEE Trans. Ind. Electron.*, vol. 69, no. 3, pp. 2610–2620, Mar. 2022.
[25] X. Wang, M. G. Taul, H. Wu, Y. Liao, F. Blaabjerg, and L. Harnefors, "Grid-synchronization stability of converter-based resources—An overview," *IEEE Open J. Ind. Appl.*, vol. 1, pp. 115–134, 2020.
[26] C. Lascu, "Sliding-mode direct-voltage control of voltage-source converters with LC filters for pulsed power loads," *IEEE Trans. Ind. Electron.*, vol. 68, no. 12, pp. 11642–11650, Dec. 2021.
[27] P. Mattavelli, "An improved deadbeat control for ups using disturbance observers," *IEEE Trans. Ind. Electron.*, vol. 52, no. 1, pp. 206–212, Feb. 2005.
[28] D. Pérez-Estévez, J. Doval-Gandoy, and J. M. Guerrero, "AC-voltage harmonic control for stand-alone and weak-grid-tied converter," *IEEE Trans. Ind. Appl.*, vol. 56, no. 1, pp. 403–421, Jan./Feb. 2020.
[29] H. Paynter, *Analysis and Design of Engineering Systems: Class Notes for MIT Course 2,751*. Cambridge, MA, USA: MIT Press, 1961.
[30] G. Franklin, J. Powell, and M. Workman, *Digital Control of Dynamic Systems*, 3rd ed. Boston, MA, USA: Addison-Wesley, 1998.
[31] A. G. Yepes, F. D. Freijedo, J. Doval-Gandoy, O. Lopez, J. Malvar, and P. Fernandez-Comesana, "Effects of discretization methods on the performance of resonant controllers," *IEEE Trans. Power Electron.*, vol. 25, no. 7, pp. 1692–1712, Jul. 2010.
[32] R. Costa-Castelló and E. Fossas, "On preserving passivity in sampled-data linear systems by using state observers," in *Proc. Eur. Control Conf.*, 2007, pp. 5276–5281.
[33] Y. Oishi, "Passivity degradation under the discretization with the zero-order hold and the ideal sampler," in *Proc. 49th IEEE Conf. Decis. Control*, 2010, pp. 7613–7617.
[34] V. Pirsto, J. Kukkola, M. Hinkkanen, and L. Harnefors, "Intersample modeling of the converter output admittance," *IEEE Trans. Ind. Electron.*, vol. 68, no. 11, pp. 11348–11358, Nov. 2021.
[35] F. Hans, M. Oeltze, and W. Schumacher, "A modified ZoH model for representing the small-signal PWM behavior in digital DC-AC converter systems," in *Proc. 45th Annu. Conf. IEEE Ind. Electron. Soc.*, 2019, pp. 1514–1520.
[36] J. Ma, X. Wang, F. Blaabjerg, L. Harnefors, and W. Song, "Accuracy analysis of the zero-order hold model for digital pulse width modulation," *IEEE Trans. Power Electron.*, vol. 33, no. 12, pp. 10826–10834, Dec. 2018.
[37] R. Rosso, X. Wang, M. Liserre, X. Lu, and S. Engelken, "Grid-forming converters: Control approaches, grid-synchronization, and future trends—A review," *IEEE Open J. Ind. App.*, vol. 2, pp. 93–109, 2021.
[38] F. Hans, W. Schumacher, S.-F. Chou, and X. Wang, "Design of multifrequency proportional–resonant current controllers for voltage-source converters," *IEEE Trans. Power Electron.*, vol. 35, no. 12, pp. 13573–13589, Dec. 2020.
[39] F. D. Freijedo, M. Ferrer, and D. Dujic, "Multivariable high-frequency input-admittance of grid-connected converters: Modeling, validation, and implications on stability," *IEEE Trans. Ind. Electron.*, vol. 66, no. 8, pp. 6505–6515, Aug. 2019.
[40] J. Mace, A. Cervone, and D. Dujic, "Enhancing the perturbation injection capabilities of grid-connected converters with asymmetric signals," *CPSS Trans. Power Electron. Appl.*, vol. 9, no. 3, pp. 345–359, Sep. 2024.
[41] A. Vidal et al., "Assessment and optimization of the transient response of proportional-resonant current controllers for distributed power generation systems," *IEEE Trans. Ind. Electron.*, vol. 60, no. 4, pp. 1367–1383, Apr. 2013.

Alvaro Morales-Muñoz (Student Member, IEEE) received the B.Sc. degree in mechanical and electrical engineering from the Universidad de Málaga, Málaga, Spain, in 2018, and the M.Sc. degree in industrial engineering from the Universidad Politécnica de Madrid, Madrid, Spain, in 2020. He is currently working toward the industrial Ph.D. degree in electronic engineering with Kiel University, Kiel, Germany, and the Huawei Nuremberg Research Center, Nuremberg, Germany.

His research interests include control methods applied to grid-connected power electronics converters, especially for renewable energy systems.

Francisco D. Freijedo (Senior Member, IEEE) received the M.Sc. degree in physics from the University of Santiago de Compostela, Santiago de Compostela, Spain, in 2002, and the Ph.D. degree in electrical engineering from the University of Vigo, Vigo, Spain, in 2009.

From 2005 to 2011, he was a Lecturer with the Department of Electronics Technology, University of Vigo. From 2011 to 2014, he was a Power Electronics Control Engineer for renewable energy applications with the Gamesa Innovation and Technology, Madrid, Spain. From 2014 to 2016, he was a Postdoctoral Researcher with the Department of Energy Technology, Aalborg University, Aalborg, Denmark. From 2016 to 2019, he was a Scientific Collaborator with the Power Electronics Laboratory, Ecole Polytechnique Federale de Lausanne, Lausanne, Switzerland. He is currently a Power Electronics Control Expert with Huawei Technologies, Shenzhen, China. His research focuses on power conversion technologies.

Dr. Freijedo is an Associate Editor for IEEE TRANSACTIONS ON INDUSTRIAL ELECTRONICS, IEEE TRANSACTIONS ON POWER ELECTRONICS, and IEEE TRANSACTIONS ON INDUSTRY APPLICATIONS.

Sante Pugliese (Member, IEEE) received the M.Sc. degree in automation engineering and the Ph.D. degree in electrical and information engineering from the Politecnico di Bari, Bari, Italy, in 2013 and 2018, respectively.

Since 2018, he has been a Postdoctoral Researcher at the Chair of Power Electronics with Kiel University, Kiel, Germany, leading the control group. From 2018 to 2019, he was Postdoc responsible in the EEMSWEA project, Medium Voltage Grid Analyzer - Mittel Spannungs Netz Analyse. In 2020, he was a Postdoc responsible in the Add-On project funded by the Bundesministerium für Wirtschaft und Energie, Berlin, Germany. His research interests include power converters and control techniques for distributed power generation systems based on renewable energies.

Dr. Pugliese is currently responsible for the SmartPowerConversion project under the Interreg Deutschland-Danmark program. He is an Associate Editor for IEEE INDUSTRY APPLICATIONS SOCIETY PUBLICATIONS.

Marco Liserre (Fellow, IEEE) received the M.Sc. and Ph.D. degrees in electrical engineering from the Politecnico di Bari, Bari, Italy, in 1998 and 2002, respectively.

Since 2012, he has been an Associate Professor with the Politecnico di Bari, and a Professor of reliable power electronics with Aalborg University, Aalborg, Denmark. Since 2013, he has been a Full Professor and holds the Chair of Power Electronics with the University of Kiel, Kiel, Germany. He has been offered and declined professorships at several universities. He has authored or coauthored more than 700 technical papers (1/3 of them in international refereed journals), one book, and seven granted patents (four with companies). These works have received more than 50 000 citations. From 2014 to 2021, he was selected as an Highly Cited Researcher in the field of Engineering (Clarivate Web of Science). Several of his students (M.Sc., Ph.D., and postdocs) are in leading positions in industry and universities worldwide. In 2023, he joined the Fraunhofer ISIT on a part-time basis as Deputy Director and Director of the new division "Electronic Energy Systems," as well as of the Kiel branch of the Fraunhofer ISIT.

Dr. Liserre is a Member of IAS, PELS, PES, and IES. He has served all these societies in various capacities. In PELS, he is Co-Editor of the IEEE OPEN ACCESS JOURNAL IN POWER ELECTRONICS and Technical Committee Chairman of the Committee on Electronic Power Grid Systems. He has co-chaired several IEEE conferences being several times Chairman. He was a recipient of 16 awards from IEEE, PCIM, and EPE-PEMC, including the prestigious 2018 IEEE-IES Mittelmann Achievement Award and the 2023 IEEE-PELS R. David Middlebrook Achievement Award. In 2023, he was the recipient of the title of "Ufficiale" by the President of the Italian Republic. In 2025, he will be Chairman of Powertech 2025 in Kiel.